DL-CFAR: a Novel CFAR Target Detection Method Based on Deep Learning

Chia-Hung Lin[1], Yu-Chien Lin[1], Yue Bai[2], Wei-Ho Chung[1], Ta-Sung Lee[1], *Fellow, IEEE*, and Heikki Huttunen[2], *Member, IEEE*
[1]Center for mmWave Smart Radar Systems and Technologies, National Chiao Tung University, Taiwan
[2]Faculty of Information Technology and Communication Sciences (ITC), Tampere University, Finland
Email: cyshlovelion@nctu.edu.tw, max821002@gmail.com, yue.bai@tuni.fi, whchung@ee.nthu.edu.tw, tslee@mail.nctu.edu.tw, heikki.huttunen@tuni.fi

***Abstract*—The well-known cell-averaging constant false alarm rate (CA-CFAR) scheme and its variants suffer from masking effect in multi-target scenarios. Although order-statistic CFAR (OS-CFAR) scheme performs well in such scenarios, it is compromised with high computational complexity. To handle masking effects with a lower computational cost, in this paper, we propose a deep-learning based CFAR (DL-CFAR) scheme. DL-CFAR is the first attempt to improve the noise estimation process in CFAR based on deep learning. Simulation results demonstrate that DL-CFAR outperforms conventional CFAR schemes in the presence of masking effects. Furthermore, it can outperform conventional CFAR schemes significantly under various signal-to-noise ratio conditions. We hope that this work will encourage other researchers to introduce advanced machine learning technique into the field of target detection.**

***Keywords*—constant false alarm rate (CFAR), target detection, deep learning, neural network.**

I. Introduction

THE core concept of target detection schemes is to evaluate the noise level in a range-Doppler (RD) map according to neighbor cells surrounding the cell under test (CUT) and set an appropriate threshold for detecting targets. The cell-averaging constant false alarm rate (CA-CFAR) [1] utilizes the arithmetic mean of power of reference cells as noise level estimates. One of its variants, namely greatest of cell-averaging CFAR (GOCA-CFAR) [2], can improve the false alarm rate of the orginal scheme. Although both schemes perform well in homogeneous scenarios, their performance degrades in multi-target scenarios based on erroneous noise level estimation. Smallest of cell-averaging CFAR (SOCA-CFAR) [3] has been proposed to improve performance in multi-target scenarios. However, it does not improve performance significantly in dense multi-target scenarios. Order-statistic CFAR (OS-CFAR) [4] can handle such problems, but it introduces significant computational complexity. Therefore, it is necessary to develop a robust scheme for multi-target scenarios with lower computational complexity. This goal was the major motivation for this study.

Recently, the authors in [5] propose exploiting deep learning techniques to improve the detection performance with CA-CFAR with a lower false alarm rate. In [6], a support vector machine model for selecting the best CFAR scheme for a given reference window is proposed. However, the performance of these schemes is only marginally better than that of conventional schemes because they simply train models to emulate the conventional ones or choose an optimal conventional scheme. We also observe that the degeneration of well-known CFAR schemes occurs at high signal-to-noise ratios (SNR) and in multi-target scenarios. In such cases, strong side-lobes associated with target returns cause overestimated noise levels, resulting in lower detection rates. Hereafter, this phenomenon is referred to as the side-lobe issue for the sake of brevity. If side-lobes can be eliminated, superior noise estimation results can be achieved.

In [7], [8], the authors employ deep learning model to tackle the denoising problem. Their works suggest that deep learning models can recognize the structured pattern and remove noise patterns in an image. Inspired by these works, we propose a novel CFAR detection scheme aided by a deep learning model called DL-CFAR. The proposed model learns the structures of targets in an RD map and eliminates those structures to acquire an RD map with pure noise, which can be used to estimate noise levels more accurately and facilitate CFAR detection that is robust in various scenarios. This paper is the first attempt to directly enhance the noise estimation process of CFAR. As a result, the proposed scheme outperforms conventional CFAR schemes significantly. Furthermore, the performance of conventional CFAR schemes is influenced by parameter settings (guard cell size, order selection). Poor parameter settings in conventional CFAR schemes may lead to significant performance decay. In contrast, no parameter settings are required for DL-CFAR. As a result, the proposed method is a practical CFAR target detection scheme for real-world implementation.

The remainder of the paper is organized as follows. Section II presents the system model. Section III describes the development of DL-CFAR. Section IV gives the simulation results. Finally, Section VI draws the conclusions.

II. System Model

Target information (i.e., range and Doppler velocity of each target relative to the observer) is acquired by performing target detection based on self-radiated returns from targets. In

978-1-7281-1220-6/19/$31.00 ©2019 IEEE

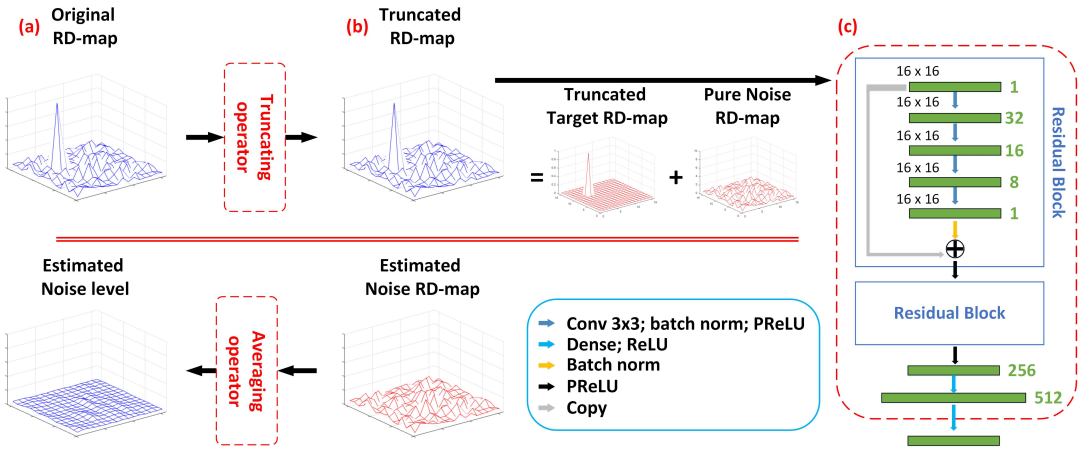

Fig. 1. (a) Overview of the proposed DL-CFAR. (b) Truncated RD map combining a truncated target RD map and pure noise RD map. The proposed neural network can remove the truncated target RD map. As a result, the output of the proposed neural network is similar to the pure noise RD map. (c) The Architecture of the proposed neural network.

frequency modulated continuous wave (FMCW) radar and orthogonal frequency division modulation radar (OFDM), time-frequency channel coefficients are exploited to derive target information. In a general form, the channel coefficient of the kth frequency and lth time sample of a target return can be represented as

$$(\mathbf{H})_{k,j} = \sum_{h=0}^{H-1} b_h e^{-2\pi f_{\mathrm{D},h} l T_\mathrm{s}} e^{-2\pi \tau_h k \Delta f} e^{j\phi_h}, \qquad (1)$$

where $\mathbf{H}$ is a channel coefficient matrix (CCM) consisting of H target returns, and T_s and Δf are the sample period and frequency spacing, respectively. b_h, $f_{\mathrm{D},h}$, τ_h, and ϕ_h are the complex amplitude, Doppler shift, round-trip time, and random phase rotation, respectively, associated with the hth target return.

Specifically, considering FMCW radar as an example, we transmit a frame composed of M chirps (a chirp is a sinusoid whose frequency increases linearly with time), then mix the transmitted and received chirps into M intermediate frequency (IF) signals in chirp-by-chirp fashion. Next, we extract N samples of the IF signal in each chirp using a predetermined sampling period. The CCM is constructed from cascading columns of these chirp-by-chirp samples, as illustrated in Fig. 2. In this case, the sampling period is T_s and the frequency spacing of the adjacent samples in each chirp is Δf.

The 2D fast Fourier transform (FFT) operation is a well-known solution for identifying sinusoids in a discrete-time signal. An RD map is generated by performing a 2D FFT on a CCM $\mathbf{H}$, which can be represented as

$$\begin{aligned} \mathrm{RDM}(n,m) &= |\text{2D FFT}(\mathbf{H})(n,m)|^2 \\ &= |\sum_{k=0}^{N-1}\sum_{l=0}^{M-1} (\mathbf{H})_{k,l} e^{j2\pi lm/M} e^{j2\pi kn/N}|^2, \end{aligned} \qquad (2)$$

where N and M are the FFT lengths in the frequency and time domains, respectively.

An RD map is composed of $N \times M$ RD bins. Maximum-ratio-combining (MRC) is achieved at RD bins for which the range and Doppler velocity of targets match both discrete sinusoidal components in both domains. Such RD bins are referred to as MRC RD bins. Note that a processing gain of $10\log_{10}(NM)$ dB can be achieved after performing the 2D FFT operation to enhance the power of target returns. Therefore, to derive target information, a CFAR detection scheme can be applied to identify peaks.

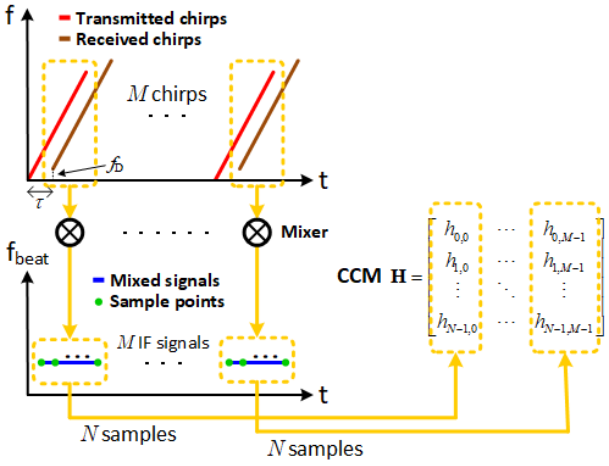

Fig. 2. Illustration of CCM generation for FMCW radar.

III. Development of DL-CFAR

In the proposed scheme, we deal with an RD map with the size of $N_\mathrm{W} \times M_\mathrm{W}$. For an RD map with a large size, we can divide it into several RD maps with the size of $N_\mathrm{W} \times M_\mathrm{W}$ such that they are processed independently. Our scheme focuses on the development of a neural network that can recognize and remove target patterns from an original RD map to obtain more accurate noise level estimations. DL-CFAR is summarized in Fig. 1. In Fig. 1 (a), an input RD map is first fed into a truncating operator as a truncated RD map. The resulting RD map is then treated as an input for

the proposed neural network. The truncated RD map can be considered as a combination of a truncated target RD map and a noise RD map, as shown in Fig. 1 (b). The proposed neural network can remove target patterns in the truncated RD map, allowing us to approximate a pure noise RD map and estimate noise levels at each RD bin in the RD map accurately.

A. Data Pre-processing

The proposed neural network must be able to handle input RD maps with various magnitudes. A conventional solution to this problem is to employ a normalization operator prior to processing by the neural network. However, the noise would be normalized to nearly zero for every RD bin in the RD map at high SNR, making it fail to update weights of the neural network properly. Therefore, we use a truncating operator to handle different RD map magnitudes. Although strong target patterns may be truncated, the proposed neural network still has the ability to recognize and remove such patterns from the RD map, demonstrated by the simulation results discussed later in this paper.

B. Architecture of the Proposed Neural Network

Fig. 1 (c) presents the architecture of the proposed neural network. The inputs for the proposed neural network are fed into several residual blocks first. In each residual block, we employ convolutional neural networks (CNNs) and each CNN layer employs kernels with dimensions of 3×3 to exploit the spatial local correlations in input RD maps. The numbers of feature maps in each layer are 32, 16, 8, and 1, respectively, and the output size for each layer in the residual block is the same as the size of the input RD map, which is $N_{\mathrm{W}} \times M_{\mathrm{W}}$. Batch normalization [9] is performed after each CNN to speed up convergence and avoid over-fitting problems. Finally, we use the parametric rectified linear unit (PReLU) [10] as an activation function to introduce non-linearity. The output of the residual block chain will be fed into two fully-connected layers. The numbers of neurons in the two layers are 512 and $N_{\mathrm{W}}M_{\mathrm{W}}$, respectively. Following these layers, we use a rectified linear unit (ReLU) as an activation function. It is noteworthy that the output of a residual block has the same size as the input of a residual block. This design was inspired by [11] and was adopted to remove target patterns step by step. Another feature of the proposed neural network is that we do not include any pooling layers in the design of neural network because we want to keep all information from an RD map to estimate noise levels precisely. The same design concept can be found in [12], [13]. The number of residual blocks is set to two. Additional residual blocks and layers do not improve performance, but they do increase computational complexity.

C. Training Method

We use end-to-end learning to train all trainable kernels and bias Θ in the neural network. An input RD map is denoted as $\mathrm{RDM} = \mathbf{T}+\mathbf{N}$, where $\mathbf{T}$ represents a pure target RD map and $\mathbf{N}$ represents a pure noise RD map. The resulting truncated RD map can be expressed as $\mathrm{RDM}_{\mathrm{T}} = \tilde{\mathbf{T}} + \mathbf{N}$, where $\tilde{\mathbf{T}}$ represents the truncated target RD map. The proposed neural network is a supervised learning algorithm and we employ the mean square error as a loss function as follows:

$$L(\Theta) = \sum_{i=1}^{D} (\mathrm{N}_i - f(\mathrm{RDM}_{\mathrm{T},i}; \Theta))^2, \tag{3}$$

where D is the total number of samples in the training dataset. During the training process, Adam [14], a gradient-decent-based optimizer, is used to update all the trainable parameters iteratively. The initial learning rate is set as 0.00005 and the batch size is set to 128. After 500 epochs, the training process is completed and the weights are recorded.

TABLE I
VALIDATION LOSS OF THE PROPOSED NEURAL NETWORK VERSUS DIFFERENT TRAINING SNR

SNR	25	26	27	28	29	30	31
Loss (e-2)	7.5	7.364	7.291	**7.290**	7.376	7.511	7.523

IV. Simulation Results and Discussion

In our simulations, we compared the proposed scheme to four well-known CFAR schemes: CA-CFAR, GOCA-CFAR, SOCA-CFAR and OS-CFAR.

To obtain a dataset for DL-CFAR, we generated RD maps with $N_{\mathrm{W}} = M_{\mathrm{W}} = 16$ according to the system model. The number of samples in the training datasets was 40000 and the numbers of samples in the validation and testing datasets were 200000. In the training dataset, single-target and two-target scenarios were considered. The two-target scenarios were designed to let the proposed neural network learn the interactions between target returns in an RD map. For the truncating operator of DL-CFAR, as a rule of thumb, the upper-bound threshold was set to 10 in this paper. All simulation results presented in this paper represent the average results for the testing dataset excluding the training and validation dataset.

A. Training SNR

Note that in this paper, SNR is defined as the SNR observed at an MRC RD bin. In an initial simulation, we determined the best training SNR for the proposed neural network. Several neural networks were trained independently using the training dataset with different SNR. We then tested those neural networks on a validation dataset including data with 21 different SNR from 19 to 39 dB and the size of each data for different SNR is 10000. The results of validation loss of the proposed neural network with different SNR are shown in Table. I. The neural network trained with SNR of 28 dB perform best because it has the lowest validation loss. The performance of neural networks trained with lower SNR decayed slightly because learning target structures in a noisy environment is challenging. However, the performance of neural networks trained with higher SNR also decayed slightly because neural networks trained in ideal (noise-free) environments do not have the ability to handle noise. This results suggest that the best training SNR is mid-range value. As a result, we employed a

neural network trained with SNR of 28 dB for the following simulations.

B. Noise Estimation Performance of DL-CFAR

Because noise level estimation is the most important part of CFAR detection schemes, we evaluated the test schemes in terms of bias and standard deviation of noise level estimation. We evaluated OS-CFAR using different orders, but only present the best two results for the sake of brevity. Table. II lists the bias and standard deviation in noise level estimation for different CFAR schemes with different SNR and numbers of targets. In high-SNR or multi-target scenarios, the biases and standard deviations of CA-CFAR and its variants (SOCA-CFAR and GOCA-CFAR) increase significantly because of the side-lobe issue. It is also revealed that although OS-CFAR has a low standard deviation, it suffer from underestimating noise level, leading to more false alarms. DL-CFAR is the most robust scheme with different SNR and number of targets since the proposed neural network can solve the side-lobe issue by eliminating target patterns from RD maps. Moreover, researches have shown that deep learning approaches can employ deeper architecture to learn and find more suitable features automatically instead of using rule-based manipulation just like what the other CFAR schemes do.

C. Performance of DL-CFAR in Single Target Scenarios

In the simulations discussed below, we aimed to discuss the trade-offs between the detection rates and false alarm rates of different CFAR schemes in single target scenarios. As a rule of thumb, a target can be successfully detected when the SNR is greater than 30 to 35 dB [15]. Fig. 3 shows the detection rates versus false alarm rates of different CFAR schemes with low SNR. CA-CFAR and its variants perform well in homogeneous scenarios. DL-CFAR outperforms all the other CFAR schemes significantly. Fig. 4 and 5 show the detection rates versus false alarm rates of different CFAR schemes with middle and high SNR. All CFAR schemes perform better when the test SNR increases because the difficulty of target detection decreases. It is noteworthy that, in the regime of low false alarm rates, the performance of DL-CFAR is clearly superior to that of other schemes. This phenomenon reveals that DL-CFAR can attain a significant improvement in detection rate even in an extremely low false alarm rate.

In conclusion, although the other CFAR schemes employ guard cells to handle the side-lobe issue, their performance drops because the fixed-size guard cells cannot handle various types of side-lobes. By employing neural networks, DL-CFAR can recognize and remove target patterns in different scenarios. As a result, the performance of DL-CFAR is superior to those of all the other CFAR schemes with different SNR.

D. Performance of DL-CFAR in Multi-target Scenarios

In this section, we evaluate different CFAR schemes in multi-target scenarios. Fig. 6 represents the detection rate versus false alarm rate for different CFAR schemes for scenarios with SNR = 20 dB and three targets. The performance of DL-CFAR exceeds that of the other CFAR schemes. When false

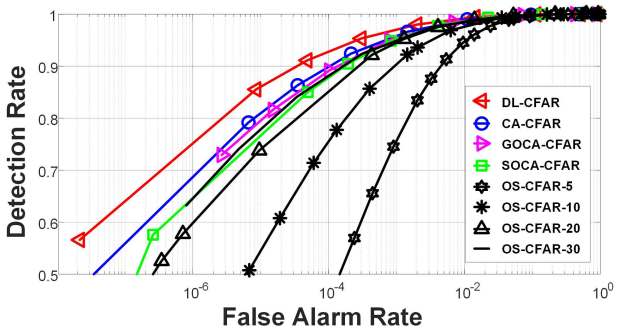

Fig. 3. Detection rate versus false alarm rate for different CFAR schemes with SNR = 20 dB (low SNR).

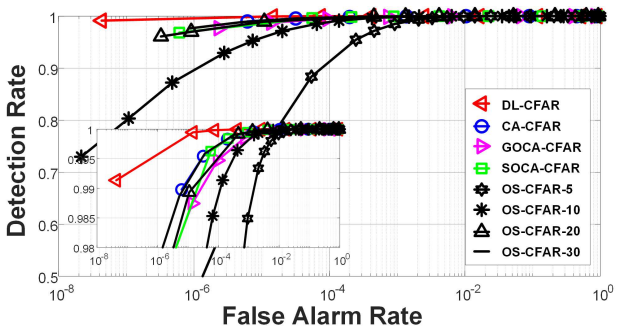

Fig. 4. Detection rate versus false alarm rate for different CFAR schemes with SNR = 25 dB (middle SNR).

alarm rate is 10^{-4}, which is an commonly adopted value, DL-CFAR outperforms the other CFAR schemes by approximately 6% in terms of detection rate. Fig. 7 shows the simulation results in four-target scenario with SNR = 20 dB. When false alarm rate is 10^{-4}, DL-CFAR has a better improvement of at least 8% in terms of detection rate. In conclusion, the performance of all CFAR schemes significantly degrades as the number of targets increases. In contrast, the performance of DL-CFAR only decreases slightly when the number of targets increases.

Although it has been revealed that some conventional CFAR schemes perform well in specific scenarios, such as CA-CFAR outperforming other conventional CFAR schemes in homogeneous scenarios, these schemes all provide poor performance

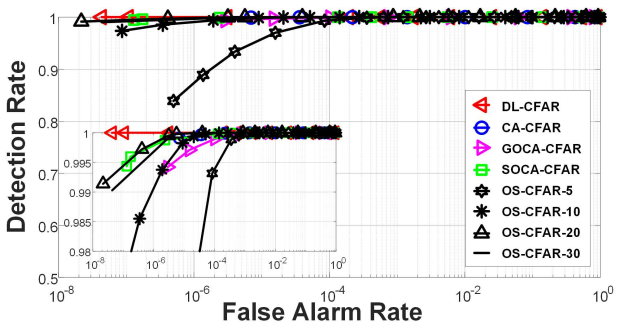

Fig. 5. Detection rate versus false alarm rate for different CFAR schemes with SNR = 30 dB (high SNR).

TABLE II
BIASES AND STANDARD DEVIATION OF DIFFERENT CFAR NOISE ESTIMATORS

SNR	no. target	OS-CFAR(5)	OS-CFAR(10)	SOCA-CFAR	GOCA-CFAR	CA-CFAR	DL-CFAR
15dB	1&2	-0.4261/0.5008	-0.3577/0.5018	-0.0705/0.5070	0.0460/0.5093	**-0.0122/0.5060**	-0.0235/0.5062
	3	-0.4179/0.5010	-0.3409/0.5011	0.0562/0.5172	0.2266/0.5305	0.1414/0.5188	**0.0455/0.5044**
	4	-0.4165/0.5010	-0.3258/0.5027	**-0.0219/0.5116**	0.2095/0.5175	0.0938/0.5097	0.0772/0.5050
25dB	1&2	-0.4210/0.5010	-0.3326/0.5031	**-0.0018/0.5068**	0.6586/1.1839	0.3284/0.7393	0.0319/0.5034
	3	-0.4515/0.5008	-0.3693/0.5021	0.0570/0.6111	1.4609/1.8700	0.7590/1.0837	**-0.0106/0.5031**
	4	-0.4022/0.5010	-0.3196/0.5018	0.2544/0.7989	1.7151/1.7360	0.9848/1.1167	**0.0098/0.5060**
35dB	1&2	-0.4388/0.5007	-0.3509/0.5007	0.0081/0.5216	5.1616/10.1267	2.5849/5.0865	**-0.0011/0.5029**
	3	-0.3593/0.5058	-0.1705/0.5257	2.3970/5.3528	13.6474/11.3075	8.0222/7.0185	**-0.0062/0.5031**
	4	-0.3447/0.5116	-0.1330/0.5637	3.9780/7.7704	17.8727/15.4677	10.9253/9.9539	**-0.0162/0.5030**

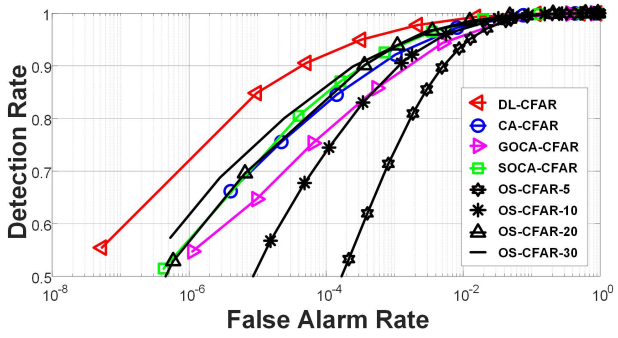

Fig. 6. Detection rate versus false alarm rate for different CFAR schemes with SNR = 20 dB and three targets.

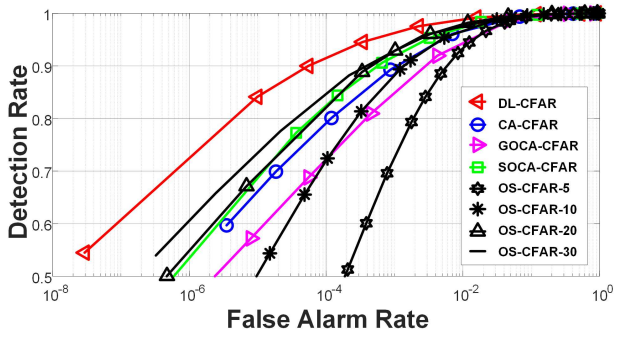

Fig. 7. Detection rate versus false alarm rate for different CFAR schemes with SNR = 20 dB and four targets.

in multi-target scenarios. In contrast, by employing neural networks, DL-CFAR always achieves the best performance in both single-target and multi-target scenarios. These results suggest that neural networks enable CFAR detection to adapt to different scenarios. It is worth investigating the robustness of DL-CFAR against various types of environmental clutter in the future.

E. Execution Time of DL-CFAR

Our simulation environment operated in MATLAB 2018b on a computer with an Intel i9-9980XE CPU, a TITAN RTX GPU, and 128GB of memory. Table. III lists the execution times of different CFAR schemes. Although CA-CFAR requires the smallest execution time, the performance of the CA-CFAR degrades significantly in multi-target scenarios. OS-CFAR is the most complex CFAR scheme and OS-CFAR performs the best among all the traditional CFAR schemes. DL-CFAR outperforms OS-CFAR in various scenarios and its execution time is comparable to that of OS-CFAR. Furthermore, neural network computations can be further accelerated by GPUs. Table. III shows that the execution time of DL-CFAR with a GPU is only slightly greater than that of CA-CFAR, which requires the smallest execution time, but DL-CFAR introduces significant performance improvements in various scenarios.

TABLE III
EXECUTION TIME OF DIFFERENT CFAR SCHEMES

Scheme	CA	GOCA	SOCA	OS	DL (CPU)	DL (GPU)
Time	7.3e-4	12e-4	12e-4	14.6e-4	14e-4	8.8e-4

V. CONCLUSION

In this paper, we proposed a novel CFAR target detection method based on deep learning technique. DL-CFAR is the first attempt to improve the noise estimation process of CFAR detection based on deep learning. Simulation results demonstrated that DL-CFAR can outperform the well-known CFAR schemes significantly with different SNR and numbers of targets. We hope this work will encourage other researchers to introduce advanced deep learning technology into the field of target detection.

ACKNOWLEDGMENT

This work was partially supported by the "Center for mmWave Smart Radar Systems and Technologies" and the "Center for Open Intelligent Connectivity" under the Featured Areas Research Center Program within the framework of the Higher Education Sprout Project by the Ministry of Education (MOE) of Taiwan, and partially supported by the Ministry of Science and Technology (MOST) of Taiwan under grant MOST 108-3017-F-009-001, MOST 108-2218-E-009-026, MOST 107-2622-8-009-020 and MOST 107-2221-E-009 -033.

REFERENCES

[1] C. R. Barrett, *Adaptive thresholding and automatic detection*. Boston, MA: Springer US, 1987, pp. 368–393. [Online]. Available: https://doi.org/10.1007/978-1-4613-1971-912

[2] V. G. Hansen and J. H. Sawyers, "Detectability loss due to "greatest of" selection in a cell-averaging cfar," *IEEE Trans. Aerosp. Electron. Syst.*, vol. AES-16, no. 1, pp. 115–118, Jan. 1980.

[3] G. V. Trunk, "Range resolution of targets using automatic detectors," *IEEE Trans. Aeros. Electron. Syst.*, vol. AES-14, no. 5, pp. 750–755, Sept. 1978.
[4] J. T. Rickard and G. M. Dillard, "Adaptive detection algorithms for multiple-target situations," *IEEE Trans. Aeros. Electron. Syst.*, vol. AES-13, no. 4, pp. 338–343, July 1977.
[5] J. Akhtar and K. E. Olsen, "A neural network target detector with partial ca-cfar supervised training," in *Int. Conf. on Radar (RADAR)*, Aug. 2018, pp. 1–6.
[6] L. Wang, D. Wang, and C. Hao, "Intelligent cfar detector based on support vector machine," *IEEE Access*, vol. 5, pp. 26 965–26 972, 2017.
[7] K. Zhang, W. Zuo, Y. Chen, D. Meng, and L. Zhang, "Beyond a gaussian denoiser: residual learning of deep cnn for image denoising," *IEEE Trans. Image Process.*, vol. 26, no. 7, pp. 3142–3155, July 2017.
[8] K. Zhang, W. Zuo, and L. Zhang, "Ffdnet: toward a fast and flexible solution for cnn-based image denoising," *IEEE Trans. Image Process.*, vol. 27, no. 9, pp. 4608–4622, Sept. 2018.
[9] S. Ioffe, and C. Szegedy,, "Batch normalization: accelerating deep network training by reducing internal covariate shift," *arXiv:1502.03167*, 2015.
[10] K. He, X. Zhang, S. Ren, and J. Sun., "Delving deep into rectifiers: surpassing human-level performance on imagenet classification," in *IEEE Int. Conf. Comput. Vis (ICCV)*, 2015, pp. 1026–1034.
[11] K. He, X. Zhang, S. Ren, and J. Sun, "Deep residual learning for image recognition," in *IEEE Conf. on Comput. Vision and Pattern Recognition (CVPR)*, June 2016, pp. 770–778.
[12] C. Wen, W. Shih, and S. Jin, "Deep learning for massive mimo csi feedback," *IEEE Wireless Commun. Lett.*, vol. 7, no. 5, pp. 748–751, Oct. 2018.
[13] D. Silver, J. Schrittwieser, K. Simonyan, I. Antonoglou, A. Huang, A. Guez, T. Hubert, L. Baker, M. Lai, A. Bolton, Y. Chen, T. Lillicrap, F. Hui, L. Sifre, G. van den Driessche, T. Graepel, and D. Hassabis, "Mastering the game of go without human knowledge," *Nature*, vol. 550, pp. 354–, Oct. 2017.
[14] D. P. Kingma and J. Ba, "Adam: A method for stochastic optimization," in *Int. Conf. Learning Representations (ICLR)*, 2014.
[15] Y. L. Sit and T. Zwick, "Automotive mimo ofdm radar: subcarrier allocation techniques for multiple-user access and doa estimation," in *11th European Radar Conf.*, Oct. 2014, pp. 153–156.